



UDC 669.295:669.018.9

<https://doi.org/10.17073/1997-308X-2024-4-69-82>

Research article

Научная статья



Structural characteristics and mechanical properties of heat-resistant TNM-B1 alloy obtained by selective laser melting from SHS powder spheroidized in thermal plasma

G. M. Markov¹ , A. A. Fadeev^{1, 2}, A. A. Skirpichnikova¹,
P. A. Loginov¹, M. G. Khomutov¹, A. V. Samokhin², E. A. Levashov¹

¹ National University of Science and Technology “MISIS”

4 Bld. 1 Leninskiy Prosp., Moscow 119049, Russia

² A. A. Baikov Institute of Metallurgy and Materials Science of the Russian Academy of Sciences

49 Leninskiy Prosp., Moscow 119334, Russia

markov.sci@gmail.com

Abstract. The TNM-B1 + Y₂O₃ alloy powders obtained by the method of self-propagating high-temperature synthesis were studied. The influence of particle processing parameters in thermal plasma, generated by a DC (direct current) arc plasma torch, on the morphology and structure of spherical particles was considered. It was established that plasma treatment significantly changes the shape of the particles and allows obtaining a product with a high degree of spheroidization (from 88 to 97 %), which depends on the plasma stream temperature, the composition of the plasma-forming gas, and the amount of processed material. Using hydrogen-containing thermal plasma, the degree of spheroidization can reach 99 %. At the same time, the concentrations of impurity oxygen decrease from 0.8 to 0.13 wt. %, nitrogen decreases by 2 times, and the concentration of hydrogen significantly drops. Studies were conducted to develop selective laser melting regimes, resulting in samples with minimal defects. The optimal volumetric energy density of the laser was 40–50 J/mm³. The gasostatic treatment process allowed achieving almost complete uniformity of the samples' structure and the absence of pores. Additionally, thermal treatment at $t = 1380$ °C and $\tau = 120$ min contributed to the transformation of the initial equiaxed structure of the alloy into a lamellar one. According to the results of thermomechanical tests under the scheme of uniaxial compression in the temperature range from 800 to 1100 °C, it was established that the alloy with a lamellar structure after selective laser melting, hot isostatic pressing, and thermal treatment has increased strength values by 80–100 MPa compared to the globular structure. The mechanical properties of the alloy with a lamellar structure at $t = 800$ °C are: modulus of elasticity $E = 115.2$ GPa, yield strength $\sigma_{0.2} = 528$ MPa, compressive strength $\sigma_u = 1148$ MPa, and at $t = 1100$ °C: $E = 48.2$ GPa, $\sigma_{0.2} = 98$ MPa, $\sigma_u = 149$ MPa.

Keywords: titanium alloys, plasma spheroidization, powder metallurgy, self-propagating high-temperature synthesis, combustion synthesis, hot isostatic pressing (HIP), mechanical properties

Acknowledgements: The work was financially supported by the Ministry of Science and Higher Education of the Russian Federation within the framework of the state assignment (project 0718-2020-0034).

For citation: Markov G.M., Fadeev A.A., Skirpichnikova A.A., Loginov P.A., Khomutov M.G., Samokhin A.V., Levashov E.A. Structural characteristics and mechanical properties of heat-resistant TNM-B1 alloy obtained by selective laser melting from SHS powder spheroidized in thermal plasma. *Powder Metallurgy and Functional Coatings*. 2024;18(4):69–82.
<https://doi.org/10.17073/1997-308X-2024-4-69-82>

Особенности структуры и механические свойства жаропрочного сплава TNM-B1, полученного селективным лазерным сплавлением из сфероидизированного в термической плазме СВС-порошка

Г. М. Марков¹, А. А. Фадеев^{1, 2}, А. А. Скирпичникова¹,
П. А. Логинов¹, М. Г. Хомутов¹, А. В. Самохин², Е. А. Левашов¹

¹ Национальный исследовательский технологический университет «МИСИС»

Россия, 119049, г. Москва, Ленинский пр-т, 4, стр. 1

² Институт металлургии и материаловедения им. А.А. Байкова Российской академии наук

Россия, 119334, г. Москва, Ленинский пр-т, 49

✉ markov.sci@gmail.com

Аннотация. Исследованы порошки из сплава TNM-B1 + Y₂O₃, полученные методом самораспространяющегося высокотемпературного синтеза. Рассмотрено влияние параметров обработки частиц в термической плазме, генерируемой электродуговым плазматроном постоянного тока, на морфологию и структуру сферических частиц. Установлено, что плазменная обработка существенно изменяет форму частиц и позволяет получить продукт с высокой степенью сфероидизации (от 88 до 97 %), которая зависит от температуры потока плазмы, состава плазмообразующего газа и количества обрабатываемого материала. При использовании водородсодержащей термической плазмы степень сфероидизации может достигать 99 %. При этом снижаются концентрации примесного кислорода с 0,8 до 0,13 мас. %, азота в 2 раза и существенно падает концентрация водорода. Проведены исследования по отработке режимов селективного лазерного сплавления, в результате чего были построены образцы с минимальным количеством дефектов. При этом оптимальная объемная плотность энергии лазера составила 40–50 Дж/мм³. Процесс газостатической обработки позволил достичь практически полной однородности структуры образцов и отсутствия пор. Дополнительно проведенная термическая обработка при $t = 1380$ °C и $\tau = 120$ мин способствовала преобразованию исходной равноосной структуры сплава в ламеллярную. По результатам термомеханических испытаний по схеме одноосного сжатия в диапазоне температур от 800 до 1100 °C установлено, что сплав с ламеллярной структурой после операций селективного лазерного сплавления, горячего изостатического прессования и термической обработки имеет повышенные на 80–100 МПа значения прочности по сравнению с глобулярной структурой. Механические свойства сплава с ламеллярной структурой составили при $t = 800$ °C: модуль упругости $E = 115,2$ ГПа, предел текучести $\sigma_{0,2} = 528$ МПа, предел прочности при сжатии $\sigma_{\text{в}} = 1148$ МПа, а при $t = 1100$ °C – $E = 48,2$ ГПа, $\sigma_{0,2} = 98$ МПа, $\sigma_{\text{в}} = 149$ МПа.

Ключевые слова: титановые сплавы, плазменная сфероидизация, порошковая металлургия, самораспространяющийся высокотемпературный синтез, синтез горением, горячее изостатическое прессование (ГИП), механические свойства

Благодарности: Работа выполнена при финансовой поддержке Министерства науки и высшего образования РФ в рамках государственного задания (проект 0718-2020-0034).

Для цитирования: Марков Г.М., Фадеев А.А., Скирпичникова А.А., Логинов П.А., Хомутов М.Г., Самохин А.В., Левашов Е.А. Особенности структуры и механические свойства жаропрочного сплава TNM-B1, полученного селективным лазерным сплавлением из сфероидизированного в термической плазме СВС-порошка. *Известия вузов. Порошковая металлургия и функциональные покрытия*. 2024;18(4):69–82. <https://doi.org/10.17073/1997-308X-2024-4-69-82>

Introduction

Heat-resistant alloys based on titanium aluminides TiAl/Ti₃Al are of significant interest for technical applications in mechanical engineering [1; 2]. They are characterized by high heat resistance, corrosion resistance, and creep resistance. Under the influence of high temperatures and aggressive environments, these alloys maintain thermodynamic stability and, in addition, have low density (~5 g/cm³), which makes their spe-

cific strength superior to that of modern nickel-based superalloys of similar purpose (~9 g/cm³) [3–5].

The primary challenges hindering the use of TiAl/Ti₃Al-based alloys in the manufacture of complex-shaped parts include high sensitivity of the phase composition to process parameters, impurities, and variations in the concentrations of alloying elements, as well as the difficulty of processing at room temperature. Producing such parts through traditional metal-

lurgical methods followed by mechanical processing involves high capital costs and significant material losses [6]. Modern additive manufacturing technologies, such as selective laser melting (SLM), can address these issues by minimizing the need for mechanical processing [4; 5]. Active research is underway to optimize the compositions and production methods of heat-resistant alloy powders [6–9].

One method for producing TiAl/Ti₃Al-based alloy powders utilizes the technology of self-propagating high-temperature synthesis (SHS) [10; 11]. The potential of this method lies in the heterogeneity scale of powder particles with increased reactive surface area due to the high speed of combustion wave propagation, allowing the production of powder materials of the required composition [12–14]. Using this technology, products from basic TiAl/Ti₃Al alloys have been manufactured [15].

The development of the SLM process opens up prospects for the creation of complex-shaped products from TiAl/Ti₃Al-based materials [5; 12]. In the SLM technology, narrow particle size distribution spherical powders, are used as raw materials, which must meet specific requirements for chemical composition, impurity content, and properties such as bulk density, flowability, granulometric composition, and sphericity.

Based on these requirements, spheroidized powders from TiAl/Ti₃Al-based alloys can be obtained using gas atomization, plasma rotating electrode process (PREP method) and plasma spheroidization technologies [16–20], which ensure rapid melt crystallization, contributing to the reduction of grain size and the formation of a homogeneous structure in the solid state. Producing such powders by gas atomization and PREP methods involves using pre-manufactured cast billets and rods, increasing the process cost [18; 21–23]. Plasma spheroidization allows the use of precursor powders as raw materials, significantly simplifying the technology. Under high temperatures and the influence of surface tension forces, particles of arbitrary shape melt, acquire a spherical shape, and crystallize. This processing method improves many powder characteristics for further use in additive technologies: it increases flowability and bulk density; reduces impurity oxygen content; and helps remove internal pores formed in the original particles [24–27].

The aim of this work was to produce spherical powders in the 10–65 μm fraction from the TNM-B1 + Y₂O₃ alloy based on titanium aluminide, to study the influence of particle processing parameters in thermal plasma generated by a DC arc plasma torch on the morphology, structure, and properties of the powders,

and to use these powders in selective laser melting technology.

Materials and methods

As the starting material, powders of a reactive mixture of pure elements were used to produce the TNM-B1 alloy modified with yttrium oxide (Y₂O₃) by the SHS method in a thermal explosion mode [14]. Pressed billets of the reactive mixture were placed in a tube furnace heated to 900 °C to initiate bulk combustion. The synthesis products were sequentially ground to a powder with particle sizes <100 μm using a jaw crusher and a planetary ball mill Activator-4M (Russia). Narrow particle size distribution spherical powders with grain sizes of 10–65 μm were obtained using an air classifier Golf-3 (Russia).

The classified powders were processed in a thermal plasma stream using a powder spheroidization unit developed by the Baikov Institute of Metallurgy and Materials Science (Moscow, Russia) [28]. The parameters for the spheroidization process of micropowders in the thermal plasma stream are as follows:

Plasma torch power (N_{pl}), kW	11–25
Plasma-forming gases	Ar, Ar + H ₂
Plasma gas flow rate ($G_{pl,g}$), m ³ /h	2.0–2.16
Plasma stream enthalpy (I_{pl}), kW·h/m ³	2.0–3.9
Precursor feed rate (G_{pr}), kg/h	0.6–2.4
Transport gas flow rate – Ar($G_{tr,g}$), m ³ /h	0.5

The plasma jet is generated by a DC arc plasma torch with a power of 30 kW and flows into a water-cooled plasma reactor with a diameter of 300 mm and a length of 1000 mm. The particles of the processed material are introduced into the plasma jet as a gas-dispersed flow using a carrier gas. During particle heating, melting occurs, and spherical shapes form due to surface tension forces. The particles then crystallize, deposit on the inner surface of the plasma reactor, and partially exit to the waste gas filtration system. A reactor wall cleaning system collects and accumulates the product in receiving hoppers.

During plasma processing of the precursor powder with a wide particle size distribution, a nanosized fraction may form due to the partial evaporation of small particles and the condensation of vapors. The presence of this fraction significantly degrades the physical and technological properties of the final product and increases oxygen and nitrogen impurities due to active oxidation of nanoparticles in contact with air. The nanosized fraction was removed from the spheroidized product by sedimentation in distilled water after ultra-

sonic treatment. The target product was dried under low vacuum conditions at $t = 150\text{ }^{\circ}\text{C}$ for 180 min.

The granulometric composition of the powders was measured by laser diffraction in a liquid medium using an ANALYSETTE 22 MicroTec plus device (FRITSCH, Germany) according to ASTM B822-17. Powder flowability was assessed using a Hall funnel (calibrated funnel diameter 2.5 mm) by the standard ASTM-B213 2017 test method. Bulk density was measured according to GOST 19440-94. Impurity oxygen content was determined by reductive melting using a TC-600 instrument (LECO, USA) according to the standard ASTM E1019-18 test method.

The construction and optimization of selective laser melting (SLM) modes were carried out on an SLM-260 setup (SLM Solutions, Germany) in an inert atmosphere. The scanning speed and power were varied in the ranges of 100–1000 mm/s and 50–300 W, respectively. To eliminate defects such as pores and microcracks, SLM samples were additionally subjected to hot isostatic pressing (HIP), and to modify the structure type after HIP, they were thermally treated (HIP + TT). The HIP process was performed on a HIRP10/26–200 setup (ABRA AG, Switzerland) at a temperature of $t = 1240\text{ }^{\circ}\text{C}$, argon pressure $P_{\text{Ar}} = 200\text{ atm}$, and isothermal holding time $\tau = 120\text{ min}$. Thermal treatment was conducted in a Termionik-T1 vacuum furnace (Russia) with a tungsten heater at $t = 1380\text{ }^{\circ}\text{C}$ and $\tau = 120\text{ min}$.

Phase composition was studied by X-ray phase (XRD) analysis on a D2 PHASER diffractometer (Bruker AXS GmbH, Germany) using CuK_α radiation in the 2θ angle range of $10\text{--}120^{\circ}$ with a step size of 0.02° and exposure of 0.6 s.

Microstructural investigations were carried out on an S-3400 N scanning electron microscope (Hitachi, Japan) with an energy-dispersive attachment NORAN System 7 X-ray Microanalysis System (Thermo Scientific, USA).

Thermomechanical tests under uniaxial compression were conducted in a vacuum ($\sim 10^{-3}\text{ Pa}$) on a Gleeble System 3800 instrument (Dynamic Systems Inc., USA). Hot deformation diagrams of samples under compressive stress were recorded in the temperature range of 800 to 1100 $^{\circ}\text{C}$ at a strain rate $d\varepsilon/dt \leq 0.001\text{ s}^{-1}$.

Results and discussion

Precursor powder structure

The SHS powder was characterized by the presence of irregularly shaped particles and consisted of $\gamma\text{-TiAl}$

and $\alpha_2\text{-Ti}_3\text{Al}$ phases [15]. According to the structural studies (Fig. 1, *a*, *b*), it has a homogeneous microstructure, which is an important condition for obtaining high-quality spheroidized powder.

As shown by laser diffraction analysis (Fig. 1, *c*), the powders have a unimodal distribution with a peak at $\sim 10\text{ }\mu\text{m}$. The quantile distribution of particles sizes D_{10} , D_{50} , and D_{90} of the powders was 24, 40, and 68 μm , respectively. Since separation in the air classifier is predominantly based on particle mass, some particles larger than 70 μm were included in the tar-

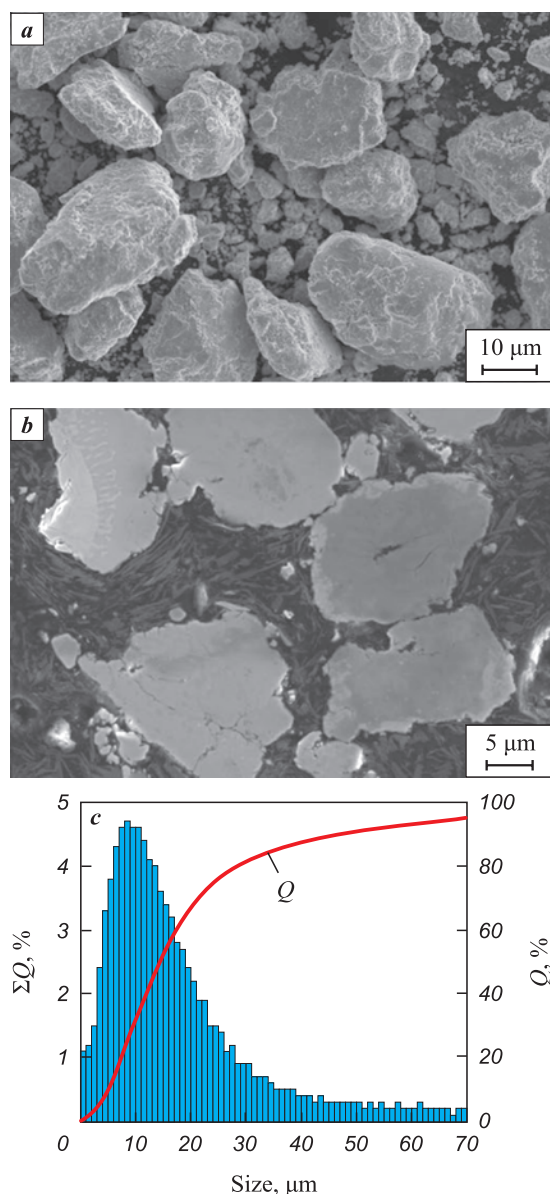


Fig. 1. Morphology (*a*), microstructure (*b*) and granulometric composition (*c*) of the TNM-B1 + 1 % Y_2O_3 powder after SHS

Рис. 1. Морфология (*a*), микроструктура (*b*) и гранулометрический состав (*c*) порошка TNM-B1 + 1 % Y_2O_3 после CBC

get fraction due to their irregular shape. The presence of a fraction smaller than 20 μm is explained by the developed surface of the particles and their mechanical interlocking. The physical and technological properties of the powders largely determine the parameters of their subsequent spheroidization in the thermal plasma stream, where a high degree (>95 %) of sphericity is required [28]. The initial SHS micropowders did not exhibit flowability, and their bulk density was 1.5 g/cm^3 .

Plasma spheroidization

Plasma spheroidization experiments were conducted with variations in the following parameters: plasma stream enthalpy, plasma-forming gas composition, and precursor powder feed rate. The main criteria for selecting the optimal plasma treatment mode for the powders were the degree of spheroidization and the minimization of the nanosized fraction in the processed powders. One significant parameter of plasma spheroidization, determining the energy contribution to the process and affecting the properties of the resulting product,

is the plasma stream enthalpy value. The properties of the spheroidized product varied depending on this parameter within the range of 2 to 3.85 $\text{kW}\cdot\text{h}/\text{m}^3$, determined by the useful power level of the DC arc plasma torch, the composition, and the flow rate of the plasma-forming gas.

At the minimum enthalpy of the argon-hydrogen plasma stream $I_{\text{pl}} = 2 \text{ kW}\cdot\text{h}/\text{m}^3$, the spheroidization degree of the product was ~73 %, which is low for powders intended for use in additive manufacturing processes (Fig. 2, *a, b*). Material evaporation with the formation of the nanosized fraction was practically absent, flowability was 57 s/50 g, and bulk density was 2.1 g/cm^3 .

Increasing $I_{\text{pl}} > 2 \text{ kW}\cdot\text{h}/\text{m}^3$ significantly raised the heat flow density to the surface of the processed powder particles, positively affecting the intensification of heating and melting particles, and consequently, increasing their spheroidization degree. However, a negative aspect of this process is the increased evaporation intensity of particles due to overheating, leading to a higher concentration of condensed

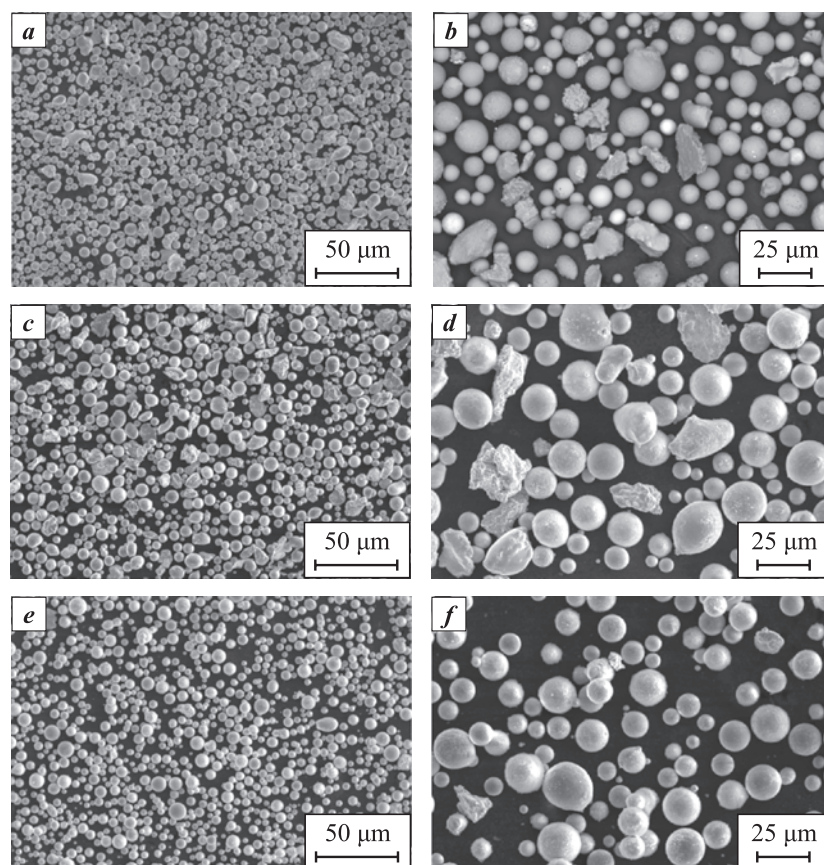


Fig. 2. Morphology of powders after spheroidization at an argon-hydrogen plasma stream enthalpy of 2 $\text{kW}\cdot\text{h}/\text{m}^3$ (*a, b*), 2.9 $\text{kW}\cdot\text{h}/\text{m}^3$ (*c, d*) and 3.85 $\text{kW}\cdot\text{h}/\text{m}^3$ (*e, f*)

Рис. 2. Морфология порошков после сфероидизации при значении энтальпии потока арговодородной плазмы 2 $\text{кВт}\cdot\text{ч}/\text{м}^3$ (*a, b*), 2,9 $\text{кВт}\cdot\text{ч}/\text{м}^3$ (*c, d*) и 3,85 $\text{кВт}\cdot\text{ч}/\text{м}^3$ (*e, f*)

nanoparticles in the spheroidized powder. Experiments showed that the maximum spheroidization degree was achieved at an argon-hydrogen plasma stream enthalpy of $I_{pl} = 3.85 \text{ kW} \cdot \text{h}/\text{m}^3$. Changing its value from 2 to $3.85 \text{ kW} \cdot \text{h}/\text{m}^3$ increased the spheroidization degree from 73 to 96 %. The nanosized fraction content increased slightly (to 2.1 wt. %), flowability reached 38 s/50 g, and bulk density increased to $2.45 \text{ g}/\text{cm}^3$.

Research found that processing the precursor powder in argon plasma produced a product with a spheroidization degree of 96 %. The presence of agglomerates and particles with satellites was noted (Fig. 3, *b*). To increase the spheroidization degree at a fixed electric arc power value, the heat transfer conditions in the “hot gas-particle” system must be changed. One possible solution is to increase the thermal conductivity of the gas medium by adding hydrogen to the plasma-forming gas. Using hydrogen-containing thermal plasma intensifies heat and mass transfer processes, reducing the heating time of processed particles, resulting in a spheroidization degree of up to 99 % (Fig. 3, *a*). It was also found that hydrogen-containing plasma creates conditions for partial reduction of the precursor powder, leading to a decrease in oxygen impurity concentration in the product.

Increasing the precursor powder feed rate requires more thermal energy from the plasma stream to heat the material, reducing the spheroidization degree. Thus, increasing the precursor feed rate from 0.6 to 2.4 kg/h decreased the spheroidization degree to 88 %, while the nanosized fraction content decreased to 2.1 wt. %. The maximum spheroidization degree (96 %) at a mini-

mal nanosized fraction content was achieved with a precursor feed rate of 1.2 kg/h. As previously shown, micropowders obtained by plasma spheroidization (Fig. 4, *a, b*) contain nano- and submicron-sized particles formed by partial evaporation of the processed material and subsequent vapor condensation during cooling of the high-temperature gas-dispersed flow. Particle content varied from 3 to 10 wt. %.

A suitable spheroidized powder for SLM technology was obtained with an Ar–H₂ plasma stream enthalpy with 3.7 vol. % hydrogen, corresponding to $I_{pl} = 3.8 \text{ kW} \cdot \text{h}/\text{m}^3$. Partial evaporation of the precursor led to the appearance of a nanosized fraction $M_{nf} = 7 \text{ wt. %}$, and the spheroidization degree reached 99 % (Fig. 4, *c–e*). The spherical particles exhibited a homogeneous globular TiAl/Ti₃Al structure with Y₂O₃ nanoparticles at grain boundaries (Fig. 4, *f*). The flowability of the resulting powders was 29 s/50 g, and bulk density increased to $2.5 \text{ g}/\text{cm}^3$. D_{10} , D_{50} , and D_{90} parameter values were 17, 29, and 50 μm, respectively, within a particle size range of 10 to 79 μm. It should be noted that processing the powder in argon plasma reduces oxygen impurities from 0.8 to 0.6 wt. %, while hydrogen-containing thermal plasma treatment, along with removing the nanosized fraction, reduces oxygen impurities to 0.3 wt. % (Fig. 5) and halves nitrogen impurities. Hydrogen content remained at 0.0025 wt. %.

Selective laser melting

The obtained powder was used to optimize the SLM modes on the SLM-260 setup (SLM Solutions,

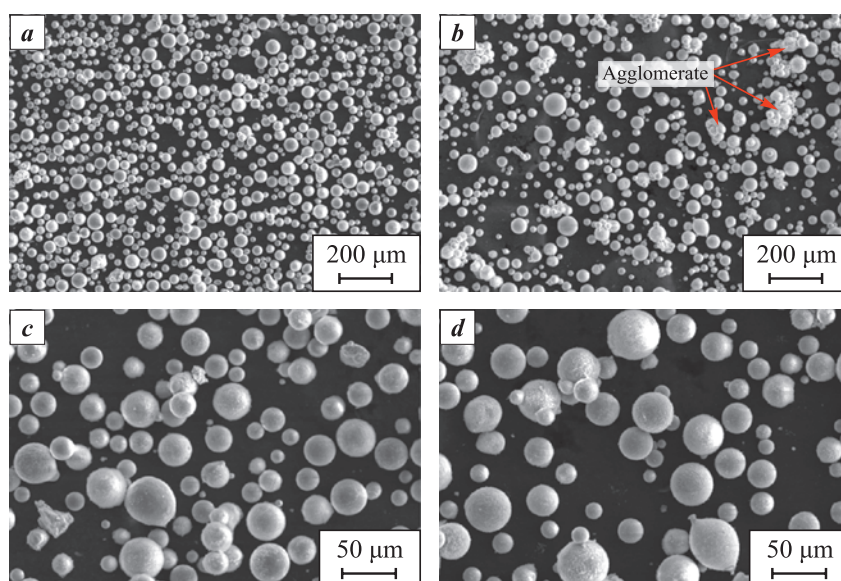


Fig. 3. Morphology of powders after spheroidization in plasma stream: Ar–H₂ (*a, c*), Ar (*b, d*)

Рис. 3. Морфология порошков после сфероидизации в плазме Ar–H₂ (*a, c*) и Ar (*b, d*)

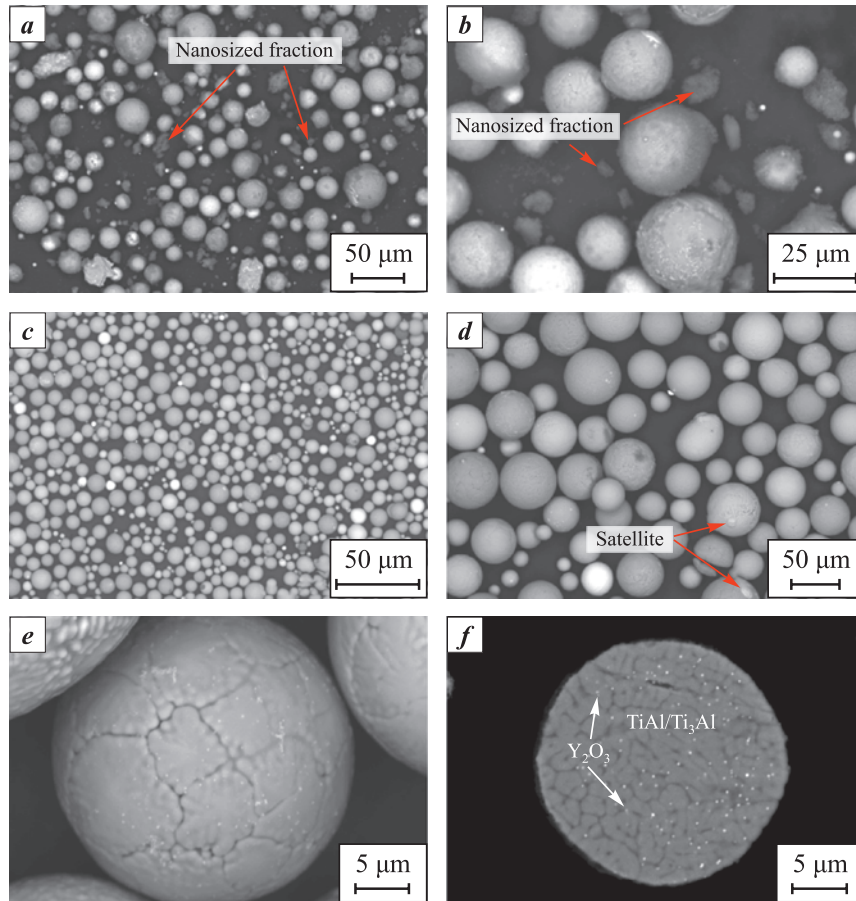


Fig. 4. Morphology of TNM-B1 + 1 % Y_2O_3 alloy powder after treatment in Ar- H_2 plasma before (a, b) and after (c, d, e) ultrasonic cleaning, and cross-section of a particle (f)

Рис. 4. Морфология порошка сплава TNM-B1 + 1 % Y_2O_3 после обработки в Ar- H_2 -плазме до (a, b) и после (c, d, e) ультразвуковой очистки и поперечный шлиф частицы (f)

Germany). The optimal ranges of the main parameters of laser synthesis were selected, considering the minimum volumetric energy density (VED) required to melt a powder layer of a given thickness, using the following formula:

$$VED = \frac{P}{vhtd},$$

where P is the laser power, W; v is the scanning speed, mm/s; h is the hatch spacing, mm; t is the powder layer thickness, mm; d is the laser beam diameter, mm.

The optimization of SLM modes using the spherical TNM-B1 + Y_2O_3 powder involved creating single tracks and evaluating the depth of melt and the presence of defects. The results of laser processing of single tracks revealed several patterns (Fig. 6). Low scanning speeds ($v < 200$ mm/s) lead to a significant increase in the depth of melt for single tracks (up to 500 μ m) regardless of the applied power, while high values of v caused significant track widening. In volumetric print-

ing, this leads to multiple remelts of adjacent tracks, and creates conditions for the formation of excessive stress and subsequent cracking of the material.

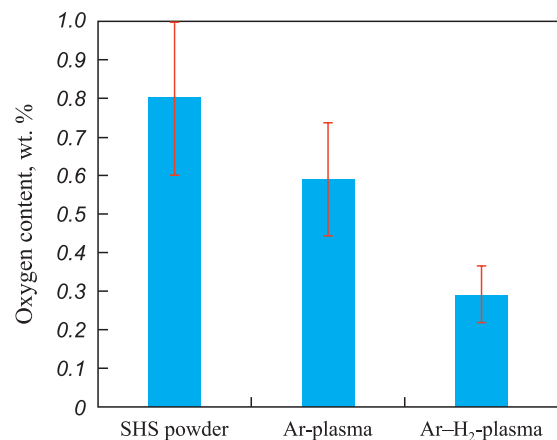


Fig. 5. Impurity oxygen content in the starting SHS powder after treatment in Ar and Ar- H_2 plasma

Рис. 5. Содержание примесного кислорода в исходном СВБ-порошке, после обработки в Ar- и Ar- H_2 -плазме

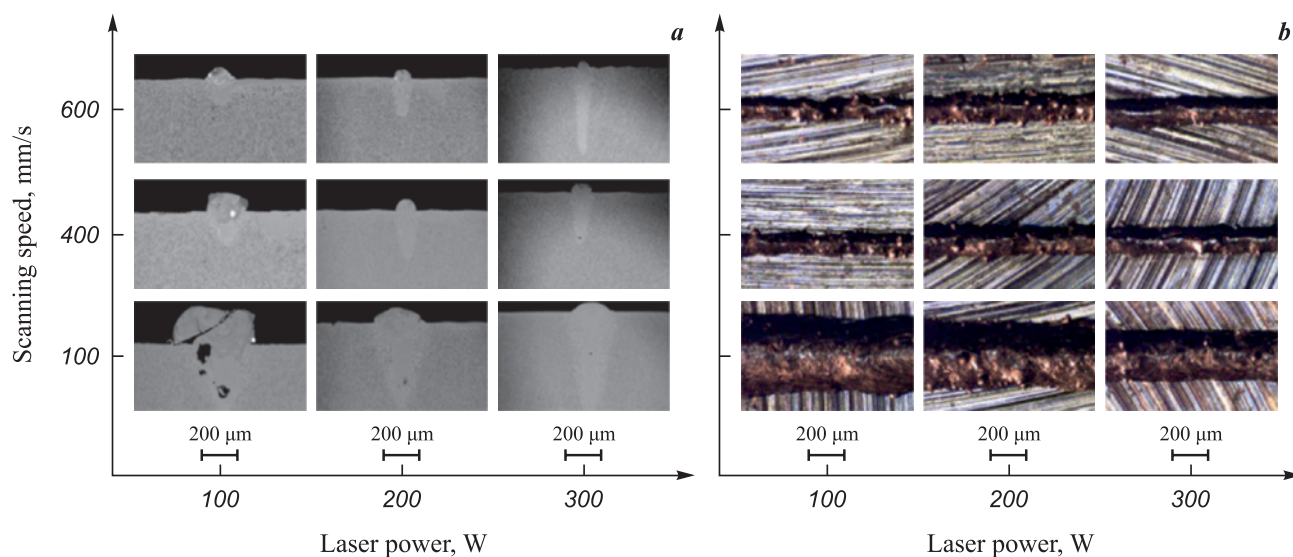


Fig. 6. SEM images of cross-section of tracks (a), and their surface images obtained by optical microscopy (b)

Рис. 6. СЭМ-изображения поперечных сечений треков (a) и снимки их поверхности, полученные методом оптической микроскопии (b)

Increasing the scanning speed from 200 to 600 mm/s reduced the number of unmelted particles on the track surface, and the track width became more uniform, ranging from 110 to 160 μm. Tracks obtained at higher scanning speeds had a smooth and uniform surface with a low number of defects. The optimal microstructure of the tracks was obtained at $v = 500 \div 600$ mm/s, and simultaneously increasing the laser power required $v > 900$ mm/s, corresponding to a volumetric energy density range of $VED = 40 \div 110$ J/mm³. Further variation of power and scanning speed for creating bulk samples was conducted within the established VED range.

Fig. 7, a shows the matrix of volumetric energy density values and a platform with bulk samples. Power variation was conducted within 70–115 W, and scan-

ning speeds in the range of 500–1000 mm/s. Samples can be divided into three groups based on characteristic defects. In Fig. 7, b, samples with warping during construction are highlighted in red, those with contour delamination in yellow, and defect-free samples in green.

For most construction modes, especially at high laser energy density (160 J/mm³), complete sample construction was not achieved. This was due to insufficient heat transfer and melt overheating, leading to warping, as well as the formation of cavities and cracks. Visual control of the SLM process for each subsequent printed layer required stopping printing for some modes due to pronounced warping of the growing samples. These modes, characterized by low laser power (70 W), ensured the formation of a dense microstructure with

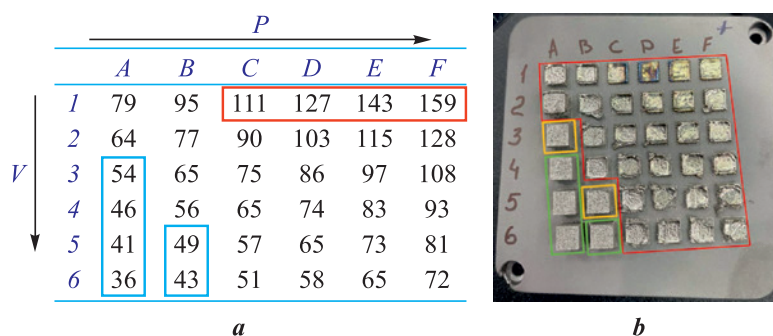


Fig. 7. SLM modes and platform with constructed samples

a – mode matrix with volumetric laser energy density values; b – image of bulk samples constructed using SLM

Рис. 7. Режимы СЛС и платформа с построенными образцами

a – матрица режимов со значениями объемной плотности энергии лазера;

b – изображение объемных образцов, построенных с помощью СЛС

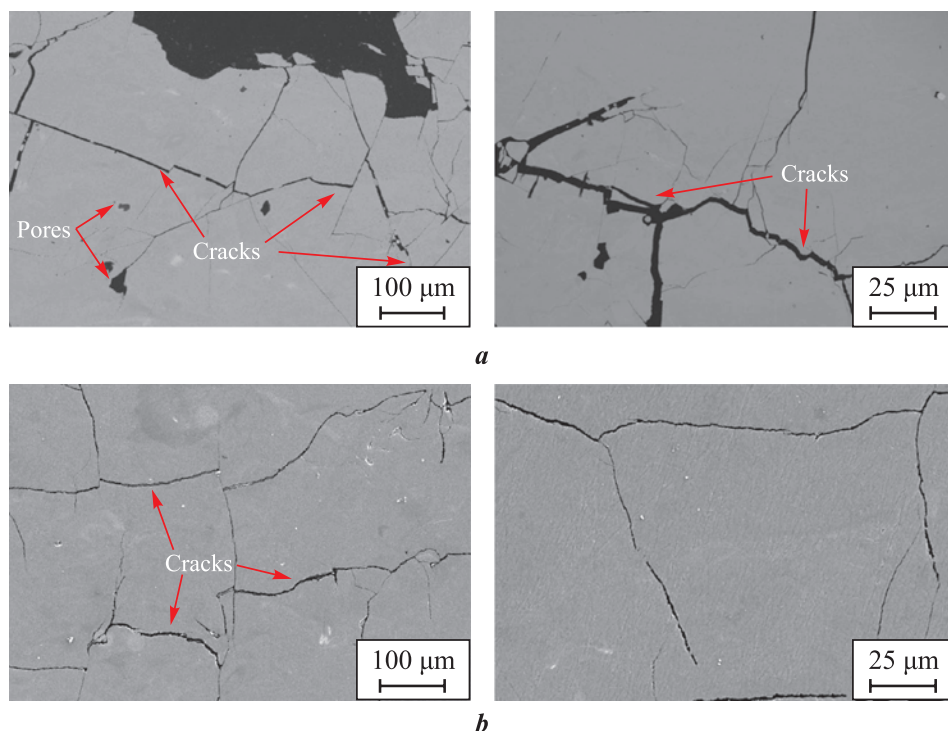


Fig. 8. Microstructures of bulk SLM samples obtained during the optimization of modes A2 (*a*) and A5 (*b*)

Рис. 8. Микроструктуры объемных СЛС-образцов, полученных при оптимизации режимов A2 (*a*) и A5 (*b*)

a uniform distribution of alloying elements. However, microcracks were present in the samples (Fig. 8, *a*), formed due to internal stress from strong temperature gradients.

As seen in Fig. 8, *b*, reducing the volumetric energy density to 50 J/mm³ and simultaneously lowering the laser power and scanning speed prevented melt pool overheating and suppressed the formation of most microcracks in the sample structures. A small number of submicron pores (<3 vol. %) were noted in these samples' structures, formed by argon entrapment in the melt pool.

Post-processing and mechanical testing

The obtained samples of the TNM-B1 + Y₂O₃ alloy with optimal structure under mode A5 (Fig. 9, *a*) were subjected to HIP and heat treatment. X-ray diffraction patterns were recorded after three types of treatment (SLM, SLM + HIP, and SLM + HIP + HT) and phase identification was conducted (Fig. 9, *b*). The TNM-B1 + Y₂O₃ alloy obtained by SLM predominantly contained the α₂-Ti₃Al phase (60 wt. %). Its concentration was 3–4 times higher than the equi-

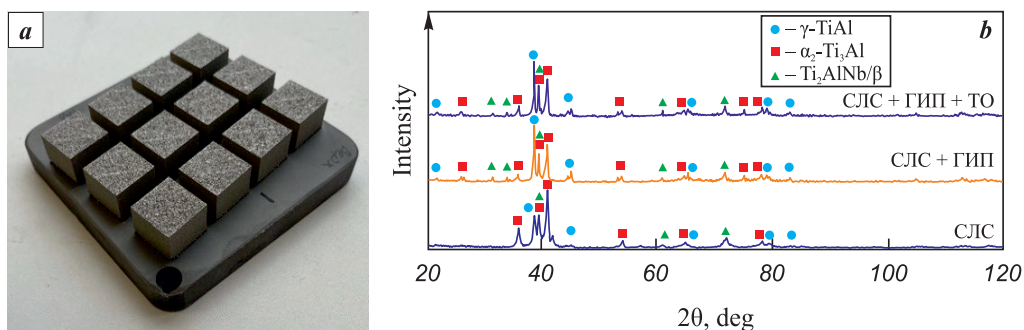


Fig. 9. Bulk samples of the TNM-B1 + Y₂O₃ alloy obtained by SLM (*a*) and X-ray diffraction patterns of this alloy after SLM, SLM + HIP, and SLM + HIP + HT (*b*)

Рис. 9. Объемные образцы из сплава TNM-B1 + Y₂O₃, полученные методом СЛС (*a*), и рентгенограммы этого сплава после СЛС, СЛС + ГИП и СЛС + ГИП + ТО (*b*)

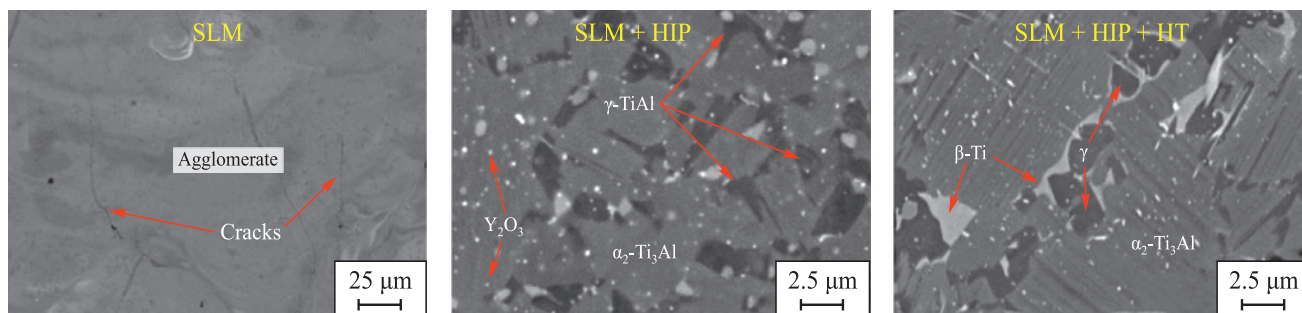


Fig. 10. Microstructures of the TNM-B1 + Y_2O_3 alloy after various types of treatment

Рис. 10. Микроструктуры сплава TNM-B1 + Y_2O_3 после различных видов обработки

librium [14]. Phase formation processes in alloys similar to TNM-B1 + Y_2O_3 are primarily controlled by the cooling rate. High cooling rates typical of SLM suppress the eutectoid reaction $\alpha \rightarrow \alpha_2 + \gamma$, resulting in an excess of the α_2-Ti_3Al [11].

HIP treatment brought the SLM TNM-B1 + Y_2O_3 alloy to an equilibrium state by transforming metastable α_2-Ti_3Al into $\gamma-TiAl$. As seen from the diffraction spectra of the SLM samples (Fig. 10), the intensity of the tetragonal $\gamma-TiAl$ phase peaks significantly increased after HIP. The $\gamma-TiAl : \alpha_2-Ti_3Al$ ratio in them was 75:20. It should be noted that both the SLM and HIP samples contained 5–7 % $\beta-Ti$ phase, which was not previously observed in this alloy obtained by HIP technology from SHS powders [15]. The SLM method for consolidation involves higher temperatures and material transition to the liquid phase, with crystallization starting with the formation of primary $\beta-Ti$ crystals according to the Ti–Al phase diagram. These $\beta-Ti$ phase grains remain in the alloy after SLM and HIP (Fig. 10).

Heat treatment (HT) did not lead to significant changes in phase composition (Fig. 9, b): the $\gamma-TiAl : \alpha_2-Ti_3Al$ ratio remained 75:20. At this stage, heating above the eutectoid transformation temperature $\alpha \rightarrow \alpha_2 + \gamma$ was carried out. As a result of slow cooling, equiaxed α -phase grains decomposed into colonies of $\gamma-TiAl : \alpha_2-Ti_3Al$ lamellae (Fig. 10).

Structural and phase changes in SLM samples occurring during HIP and HT undoubtedly affect the properties of the TNM-B1 + Y_2O_3 alloy. Fig. 11 shows deformation diagrams in the “true stress – logarithmic strain” coordinates for samples obtained under SLM mode A5, SLM + HIP, and SLM + HIP + HT. The porosity of the samples after HIP and HIP + HT did not exceed 1%. It was found that the obtained properties strongly depend on the test temperature. All deformation curves exhibit a pronounced maximum corresponding to the compressive strength and indicating the deformation hardening of the samples. All curves have a second section where deformation increases as stress decreases. This effect is explained by dynamic

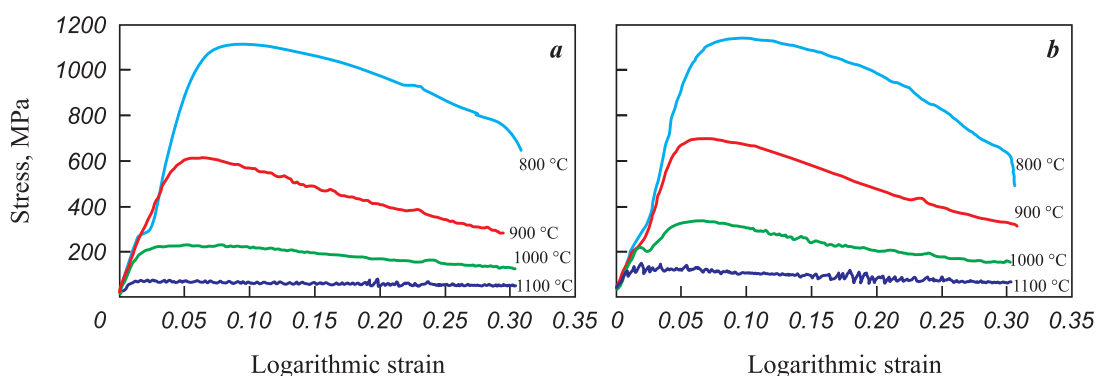


Fig. 11. Deformation diagrams under uniaxial compression in the coordinates “true stress – logarithmic strain” for SLM samples of the TNM-B1 + Y_2O_3 alloy

a – SLM + HIP; b – SLM + HIP + HT

Рис. 11. Диаграммы деформации, реализованной по схеме одноосной осадки, в координатах «истинные напряжения – логарифмическая деформация» для СЛС-образцов из сплава TNM-B1 + Y_2O_3

a – СЛС + ГИП; b – СЛС + ГИП + ТО

Mechanical properties of TNM-B1 + Y₂O₃ alloy after SLM and heat treatment (SLM mode A5)**Механические свойства сплава TNM-B1 + Y₂O₃ после СЛС и дополнительной термической обработки (режим СЛС А5)**

<i>t</i> , °C	<i>E</i> , GPa	$\sigma_{0.2}$, MPa	σ_u , MPa
Sample after SLM + HIP			
800	96.0	522	1128
900	88.0	330	622
1000	82.2	175	253
1100	73.5	94	80
Sample after SLM + HIP + HT			
800	115.2	528	1148
900	68.3	308	703
1000	54.5	181	347
1100	48.2	98	149

recrystallization or dynamic recovery and relaxation of crystal lattice defects.

Mechanical properties (elastic modulus *E*, yield strength $\sigma_{0.2}$, ultimate compressive strength σ_u) of the TNM-B1 + Y₂O₃ alloy after HIP and HIP + HT were determined using deformation diagrams (in the elastoplastic transition region). The $\sigma_{0.2}$ values of the obtained samples at 800 °C are comparable to those of cast TNM-B1 alloys ($\sigma_{0.2} = 400\div530$ MPa), and the σ_u value increased by 150–200 MPa compared to cast alloys ($\sigma_u = 880\div1000$ MPa), due to the finer grain structure [29; 30] (see Table).

HT of the TNM-B1 + Y₂O₃ alloy samples after SLM + HIP increases σ_u by 20–100 MPa due to the formation of a lamellar microstructure. The strengthening effect is more noticeable at high test temperatures (900 to 1100 °C).

Conclusions

1. Powders of the 10–65 μm fraction with a high degree of particle spheroidization (up to 99 %) were obtained from SHS powders of the TNM-B1 + Y₂O₃ alloy. The influence of particle processing parameters in thermal plasma generated by a DC plasma torch was studied. It was found that this leads to significant changes in particle morphology and the production of a product with a high degree of spheroidization ranging from 88 to 97 %, depending on plasma stream enthalpy, plasma-forming gas composition, and precursor feed rate. At the maximum spheroidization degree, partial precursor evaporation was noted, leading to the formation of up to 7 wt. % of the nanosized fraction.

2. It was established that using hydrogen-containing thermal plasma increases the spheroidization degree of the product up to 99 %. At the same time, increasing the precursor feed rate from 0.6 to 2.4 kg/h decreases the spheroidization degree from 97 to 88 %. When processing powder in hydrogen-containing thermal plasma, the impurity oxygen concentration decreases from 0.8 to 0.13 wt. %, nitrogen impurities are halved, and hydrogen concentration decreases by an order of magnitude.

3. Experiments to optimize the SLM process identified regimes that allow building preforms with minimal defects and residual porosity. The best samples were obtained at a volumetric laser energy density of 40–50 J/mm³ (laser power around 60 W) and a scanning speed above 900 mm/s.

4. The influence of post-processing (HIP and HT) on the structure, phase composition, and mechanical properties of SLM samples from the TNM-B1 + Y₂O₃ alloy was studied. After HIP, the samples had nearly zero porosity with complete healing of structural defects, and additional thermal treatment ensured the transformation of the alloy's equiaxed structure into a lamellar one.

5. Thermomechanical tests under uniaxial compression in the temperature range of 800 to 1100 °C revealed that the alloy with a lamellar structure in the SLM + HIP + HT state has increased strength values by 80–100 MPa. The best samples had the following properties at *t* = 800 °C: *E* = 115.2 GPa, $\sigma_{0.2}$ = 528 MPa, σ_u = 1148 MPa, and at 1100 °C: *E* = 48.2 GPa, $\sigma_{0.2}$ = 98 MPa, σ_u = 149 MPa.

References / Список литературы

1. Liu B., Liu Yo. Powder metallurgy titanium aluminide alloys. *Titanium powder Metallurgy. Science, Technology and Applications*. 2015;27:515–531.
<https://doi.org/10.1016/B978-0-12-800054-0.00027-7>
2. Gupta R.K., Pant B. Titanium aluminides. Intermetallic matrix composites. *Properties and Applications*. 2018;4:71–93.
<https://doi.org/10.1016/B978-0-85709-346-2.00004-2>
3. Niu H.Z., Chen X.J., Chen Y.F., Zhao S., Liu G.H., Zhang D.L. Microstructural stability, phase transformation and mechanical properties of a fully-lamellar microstructure of a Mo-modified high-Nb γ -TiAl alloy. *Materials Science and Engineering: A*. 2020;784:139313.
<https://doi.org/10.1016/j.msea.2020.139313>
4. Kartavykh A.V., Tcherdyntsev V.V., Gorshenkov M.V., Kaloshkin S.D. Microstructure engineering of TiAl-based refractory intermetallics within power-down directional solidification process. *Journal of Alloys and Compounds*. 2014;586:180–183.
<https://doi.org/10.1016/j.jallcom.2012.10.175>

5. Rittinghaus S.K., Zielinski J. Influence of process conditions on the local solidification and microstructure during laser metal deposition of an intermetallic TiAl alloy (GE4822). *Metallurgical and Materials Transactions: A*. 2021;52(3):1106–1116.
<https://doi.org/10.1007/s11661-021-06139-2>
6. Zhang S.Z., Zhang C.J., Du Z.X., Hou Z.P., Lin P., Kong F.T., Chen Y.Y. Deformation behavior of high Nb containing TiAl based alloy in $\alpha + \gamma$ two phase field region. *Materials & Design*. 2016;90:225–229.
<https://doi.org/10.1016/j.matdes.2015.10.080>
7. Nazarova T.I., Imayev V.M., Imayev R.M., Fecht H.J. Study of microstructure and mechanical properties of Ti–45Al–(Fe,Nb) (at.%) alloys. *Intermetallics*. 2017;82: 26–31. <https://doi.org/10.1016/j.intermet.2016.11.009>
8. Knörlein J., Franke M.M., Schloffer M., Berger T., Körner C. Microstructure and mechanical properties of additively manufactured γ -TiAl with dual microstructure. *Intermetallics*. 2023;161:107978.
<https://doi.org/10.1016/j.intermet.2023.107978>
9. Imayev V., Gaisin R., Rudskoy A., Nazarova T., Shaimardanov R., Imayev R. Extraordinary superplastic properties of hot worked Ti–45Al–8Nb–0.2C alloy. *Journal of Alloys and Compounds*. 2016; 663:217–224.
<https://doi.org/10.1016/j.jallcom.2015.11.228>
10. Taguchi K., Ayada M., Ishihara K.N., Shingu P.H. Near-net shape processing of TiAl intermetallic compounds via pseudoHIP-SHS route. *Intermetallics*. 1995;3(2):91–98.
[https://doi.org/10.1016/0966-9795\(95\)92673-N](https://doi.org/10.1016/0966-9795(95)92673-N)
11. Busurina M.L., Umarov L.M., Kovalev I.D., Sachkova N.V., Busurin S.M., Vadchenko S.G., Sychev A.E. Features of structure and phase formation in the Ti–Al–Nb system in the thermal explosion mode. *Combustion, Explosion and Shock Waves*. 2016;52(6):659–664.
<https://doi.org/10.15372/FGV20160605>
 Бусурина М.Л., Умаров Л.М., Ковалев И.Д., Сачкова Н.В., Бусурин С.М., Вадченко С.Г., Сычев А.Е. Особенности структуро- и фазообразования в системе Ti–Al–Nb в режиме теплового взрыва. *Физика горения и взрыва*. 2016;52(6):44–50.
<https://doi.org/10.1134/S0010508216060058>
12. Ismaeel A., Wang C. Effect of Nb additions on microstructure and properties of γ -TiAl based alloys fabricated by selective laser melting. *Transactions of Nonferrous Metals Society of China*. 2019;29(5):1007–1016.
[https://doi.org/10.1016/S1003-6326\(19\)65009-0](https://doi.org/10.1016/S1003-6326(19)65009-0)
13. Glenn E.B., Ebrahimi F., Manuel M.V. High temperature deformation of Ti–Al–Nb–Cr–Mo alloy with ultrafine microstructure. *Intermetallics*. 2014;49:132–137.
<https://doi.org/10.1016/j.intermet.2014.01.013>
14. Loginov P.A., Kaplanskii Y.Y., Markov G.M., Patsera E.I., Vorotilo K.V., Korotitskiy A.V., Shvyndina N.V., Levashov E.A. Structural and mechanical properties of Ti–Al–Nb–Mo–B alloy produced from the SHS powder subjected to high-energy ball milling. *Materials Science and Engineering: A*. 2021;814:141153.
<https://doi.org/10.1016/j.msea.2021.141153>
15. Loginov P.A., Markov G.M., Korotitskiy A.V., Levashov E.A. Compressive creep behavior of powder metallurgy manufactured Y_2O_3 -reinforced TNM-B1 TiAl alloy with equiaxed and lamellar microstructure. *Materials Characterization*. 2023;205:113367.
<https://doi.org/10.1016/j.matchar.2023.113367>
16. Polozov I., Razumov N., Makhmutov T., Silin A., Kim A., Popovich A. Synthesis of titanium orthorhombic alloy spherical powders by mechanical alloying and plasma spheroidization processes. *Materials Letters*. 2019;256:126615.
<https://doi.org/10.1016/j.matlet.2019.126615>
17. Tong B., Lu X., Liu C.C., Wang L.N., Qu X.H. Fabrication of micro-fine spherical high Nb containing TiAl alloy powder based on reaction synthesis and RF plasma spheroidization. *Powder Technology*. 2015;283:9–15.
<https://doi.org/10.1016/j.powtec.2015.04.062>
18. Yang W., Li M., Su S., Xiao S., Chen Y. Effects of carbon addition on the microstructure and mechanical property of in-situ reinforced TiAl matrix composite powders produced by plasma rotating electrode process. *Journal of Materials Research and Technology*. 2023;27:5204–5218.
<https://doi.org/10.1016/j.jmrt.2023.10.318>
19. Polozov I., Sufiarov V., Kantyukov A., Razumov N., Goncharov I., Makhmutov T., Silin A., Kim A., Starikov K., Shamshurin A. Microstructure, densification, and mechanical properties of titanium intermetallic alloy manufactured by laser powder bed fusion additive manufacturing with high-temperature preheating using gas atomized and mechanically alloyed plasma spheroidized powder. *Additive Manufacturing*. 2020;34:101374.
<https://doi.org/10.1016/J.ADDMA.2020.101374>
20. Tsvetkov Y.V., Samokhin A.V., Alekseev N.V., Fadeev A.A., Sinaiskii M.A., Levashov E.A., Kaplanskii Y.Y. Plasma spheroidization of micropowders of a heat-resistant alloy based on nickel monoaluminide. *Doklady Chemistry*. 2018; 483:312–317.
<https://doi.org/10.1134/S0012500818120030>
21. Sista K.S., Moon A.P., Sinha G.R., Pirjade B.M., Dwarpudi S. Spherical metal powders through RF plasma spheroidization. *Powder Technology*. 2022;400:117225.
<https://doi.org/10.1016/j.powtec.2022.117225>
22. Li Q., Zhang L., Wei D., Ren S., Qu X. Porous Nb-Ti based alloy produced from plasma spheroidized powder. *Results in Physics*. 2017; 7:1289–1298.
<https://doi.org/10.1016/j.rinp.2017.03.026>
23. Sheng Y.W., Guo Z.M., Hao J.J., Yang D.H. Effect of spheroidization of Ti–6Al–4V powder on characteristics and rheological behaviors of gelcasting slurry. *Procedia Engineering*. 2012;36:299–306.
<https://doi.org/10.1016/j.proeng.2012.03.044>
24. Kenel C., Leinenbach C. Influence of Nb and Mo on microstructure formation of rapidly solidified ternary Ti–Al–(Nb, Mo) alloys. *Intermetallics*. 2016;69:82–89.
<https://doi.org/10.1016/j.intermet.2015.10.018>
25. Zhang S.Z., Song Z.W., Han J.C., Zhang C.J., Lin P., Zhu D.D., Kong F.T., Chen Y.Y. Effect of 2–6 at.% Mo addition on microstructural evolution of Ti–44Al alloy. *Journal of Materials Science & Technology*. 2018;34(7):1196–1204.
<https://doi.org/10.1016/j.jmst.2017.10.012>


26. Zhou Y.H., Li W.P., Zhang L., Zhou S.Y., Jia X., Wang D.W., Yan M. Selective laser melting of Ti–22Al–25Nb intermetallic: Significant effects of hatch distance on microstructural features and mechanical properties. *Journal of Materials Processing Technology*. 2020;276:116398. <https://doi.org/10.1016/j.jmatprotec.2019.116398>
27. Polozov I., Gracheva A., Popovich A. Processing, microstructure, and mechanical properties of laser additive manufactured Ti₂AlNb-based alloy with carbon, boron, and yttrium microalloying. *Metals*. 2022;12(8):1304. <https://doi.org/10.3390/met12081304>
28. Samokhin A.V., Fadeev A.A., Kirpichev D.E., Alekseev N.V., Berestenko V.I., Astashov A.G., Zavertyaev I.D. Plasma installation for spheroidization of metal powders in a thermal plasma flow. RF Patent № RU2756327C1 (RF). 2021.
- Самохин А.В., Фадеев А.А., Кирпичев Д.Е., Алексеев Н.В., Берестенко В.И., Астахов А.Г., Завертяев И.Д. Плазменная установка для сфероидизации металлических порошков в потоке термической плазмы. Патент № RU2756327C1 (РФ). 2021.
29. Yang G., Xu X., Sun T., Xu S., Gui W., Zeng J., Mu Y., Liang Y., Lin J. A refined fully lamellar TiAl alloy extruded at α -phase region: Microstructure and mechanical properties. *Materials Science and Engineering: A*. 2023;888:145804. <https://doi.org/10.1016/j.msea.2023.145804>
30. Weisheit A., Rittinghaus S.K., Dutta A., Majumdar J.D. Studies on the effect of composition and pre-heating on microstructure and mechanical properties of direct laser clad titanium aluminide. *Optics and Lasers in Engineering*. 2020;131:106041. <https://doi.org/10.1016/j.optlaseng.2020.106041>

Information about the Authors




Сведения об авторах

Georgy M. Markov – Junior Research Scientist of the Laboratory “In situ Diagnostics of Structural Transformations” of Scientific-Educational Center of Self Propagating High Temperature Synthesis (SHS-Center) of MISIS-ISMAN, National University of Science and Technology “MISIS” (NUST MISIS)

 **ORCID:** 0000-0001-7285-7888

 **E-mail:** markov.sci@gmail.com

Andrey A. Fadeev – Cand. Sci. (Eng.), Senior Research Scientist of the Laboratory “Plasma Processes in Metallurgy and Materials Processing” of Baikov Institute of Metallurgy and Materials Science of RAS; Scientific Project Engineer of NUST MISIS

 **ORCID:** 0000-0003-2147-1787

 **E-mail:** fadeev@imet.ac.ru

Anastasia A. Skirpichnikova – Research Assistant of SHS-Center of MISIS-ISMAN

 **ORCID:** 0009-0002-1664-7039


 **E-mail:** skirpichnikova@internet.ru

Pavel A. Loginov – Cand. Sci. (Eng.), Senior Lecturer of the Department of Powder Metallurgy and Functional Coatings (PM&FC) of NUST MISIS; Senior Research Scientist of the Laboratory “In situ Diagnostics of Structural Transformations” of SHS-Center of MISIS-ISMAN

 **ORCID:** 0000-0003-2505-2918

 **E-mail:** pavel.loginov.misis@list.ru


Maxim G. Khomutov – Cand. Sci. (Eng.), Senior Research Scientist of the Laboratory of hybrid additive technologies NUST MISIS

 **ORCID:** 0000-0002-7701-1600


 **E-mail:** khomutov@isis.ru

Andrey V. Samokhin – Cand. Sci. (Eng.), Lead Research Scientist, Head of the Laboratory “Plasma Processes in Metallurgy and Materials Processing” of Baikov Institute of Metallurgy and Materials Science of RAS

 **ORCID:** 0000-0002-1708-5501


 **E-mail:** samokhin@imet.ac.ru

Evgeny A. Levashov – Dr. Sci. (Eng.), Prof., Academic of the Russian Academy of Natural Science, Head of the Department of PM&FC of NUST MISIS; Head of SHS-Center of MISIS-ISMAN

 **ORCID:** 0000-0002-0623-0013

 **E-mail:** levashov@shs.misis.ru

Георгий Михайлович Марков – мл. науч. сотрудник лаборатории «In situ диагностика структурных превращений» Научно-учебного центра (НУЦ) СВС МИСИС-ИСМАН, Национальный исследовательский технологический университет «МИСИС» (ННТУ МИСИС)

 **ORCID:** 0000-0001-7285-7888


 **E-mail:** markov.sci@gmail.com

Андрей Андреевич Фадеев – к.т.н., ст. науч. сотрудник лаборатории «Плазменные процессы в металлургии и обработке материалов» Института металлургии и материаловедения им. А.А. Байкова Российской академии наук (ИМЕТ РАН); инженер научного проекта ННТУ МИСИС

 **ORCID:** 0000-0003-2147-1787

 **E-mail:** fadeev@imet.ac.ru

Анастасия Алексеевна Скупичникова – лаборант-исследователь НУЦ СВС МИСИС-ИСМАН

 **ORCID:** 0009-0002-1664-7039

 **E-mail:** skirpichnikova@internet.ru

Павел Александрович Логинов – к.т.н., ст. преподаватель кафедры «Порошковая металлургия и функциональные покрытия» (ПМиФП) ННТУ МИСИС; ст. науч. сотрудник лаборатории «In situ диагностика структурных превращений» НУЦ СВС МИСИС-ИСМАН

 **ORCID:** 0000-0003-2505-2918

 **E-mail:** pavel.loginov.misis@list.ru

Максим Геннадьевич Хомутов – к.т.н., ст. науч. сотрудник лаборатории гибридных аддитивных технологий ННТУ МИСИС

 **ORCID:** 0000-0002-7701-1600

 **E-mail:** khomutov@isis.ru

Андрей Владимирович Самохин – к.т.н., вед. науч. сотрудник, зав. лабораторией «Плазменные процессы в металлургии и обработке материалов» ИМЕТ РАН

 **ORCID:** 0000-0002-1708-5501

 **E-mail:** samokhin@imet.ac.ru

Евгений Александрович Левашов – д.т.н., акад. РАЕН, профессор, зав. кафедрой ПМиФП ННТУ МИСИС; директор НУЦ СВС МИСИС-ИСМАН

 **ORCID:** 0000-0002-0623-0013

 **E-mail:** levashov@shs.misis.ru

Contribution of the Authors



Вклад авторов

G. M. Markov – defined the research objectives, prepared the starting materials, conducted experiments, and wrote the article.

A. A. Fadeev – conducted experiments on plasma spheroidization, participated in result discussions, and edited the article.

A. A. Skirpichnikova – participated in obtaining the starting materials.

P. A. Loginov – defined the research objectives, participated in result discussions, and revised the article.

M. G. Khomutov – conducted thermomechanical testing and participated in result discussions.

A. V. Samokhin – conceptualized and reviewed the article, participated in result discussions.

E. A. Levashov – conceptualized the research, edited the article text, and participated in result discussions.

Г. М. Марков – определение цели работы, подготовка исходных материалов, проведение экспериментов, написание текста статьи.

А. А. Фадеев – проведение экспериментов по плазменной сфероидизации, участие в обсуждении результатов, редактирование статьи.

А. А. Скирпичникова – участие в получении исходных материалов.

П. А. Логинов – определение цели работы, участие в обсуждении результатов, корректировка статьи.

М. Г. Хомутов – проведение термомеханических испытаний, участие в обсуждении результатов.

А. В. Самохин – концептуализация и проверка статьи, участие в обсуждении результатов.

Е. А. Левашов – концептуализация проводимых исследований, редактирование текста статьи, участие в обсуждении результатов.

Received 12.04.2024

Revised 27.06.2024

Accepted 28.06.2024

Статья поступила 12.04.2024 г.

Доработана 27.06.2024 г.

Принята к публикации 28.06.2024 г.